Faraday Discussions

Accepted Manuscript

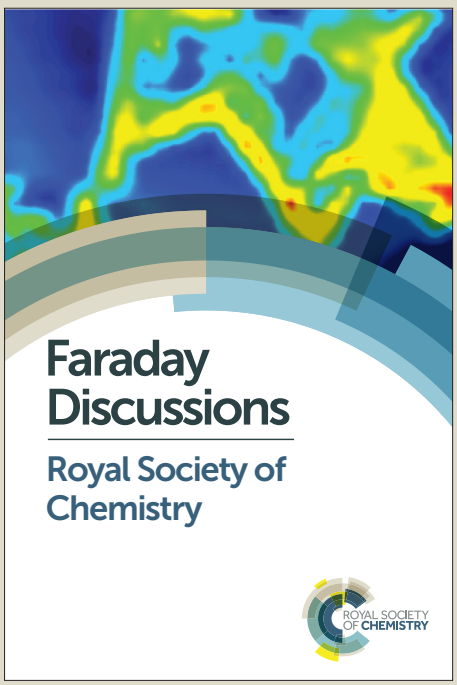

This article can be cited before page numbers have been issued, to do this please use: V. K. Deckert, T. Deckert-Gaudig, M. Diegel, I. Goetz, L. Langelueddecke, H. Schneidewind, G. Sharma, P. Singh, M. Zeisberger, Z. Zhang, P. Singh and S. Trautmann, *Faraday Discuss.*, 2015, DOI: 10.1039/C5FD00031A.

Faraday Discussions
REVIEW www.rsc.org/xxxxxx | XXXXXXXX

Spatial Resolution in Raman Spectroscopy

View Article Online
DOI: 10.1039/C5FD00031A

Volker Deckert,[a,b*] Tanja Deckert-Gaudig[a], Marco Diegel[a], Isabell Götz[a], Lucas Langelüddecke[b], Henrik Schneidewind[a], Gaurav Sharma[b], Prabha Singh[b], Pushkar Singh[a], Steffen Trautmann[a], Matthias Zeisberger[a], and Zhenglong Zhang[a]

DOI: 10.1039/b000000x [DO NOT ALTER/DELETE THIS TEXT]

This article is intended to set the scope of the meeting, in particular for the high spatial resolution section.

1 Introduction

A constant motivation to develop advanced technologies addressing temporal and spatial resolution is the investigation of structural changes of a single molecule while it is reacting. The dream is to follow a bond breakage or bond formation of a single selected molecule with a method that provides structural sensitivity, time resolution, and local specificity. Presently, such a combined technique is not yet available, however, regarding each single requirement of the mentioned list tremendous progress has been made over the last decades.

This overview will specifically address spatial resolution aspects that are required to address, if not a single molecule, at least a sample volume that is small enough to distinct the target structure from the background. The 2014 Chemistry Nobel prize awarded to Moerner, Hell, and Betzig, highlighted the importance of high resolution techniques specifically for biochemical applications. While the awarded fluorescence approach is certainly extremely useful whenever dye labelling is possible and no interference with the function of the target system is expected, in particular for smaller molecular systems such a labelling is not practical or even impossible. In such cases vibrational spectroscopy techniques can be used, often at the cost of lower sensitivity, however, as structural information is obtained directly no labelling is required and sample preparation becomes easier. In this article we will solely present the high lateral resolution aspects of Raman spectroscopy, many of those aspects can easily be applied to infrared absorption spectroscopy if the specific factors of the particular wavelength range are considered. As mentioned before the sensitivity of fluorescence label techniques easily allows the investigation of single molecules. With normal Raman scattering this is not possible as the scattering cross sections are several orders of magnitude lower compared to fluorescence. Since the mid 1970's a method exists to enhance the Raman signals considerably.[1-3] By using roughened noble metal surfaces or noble metal nanoparticles an enhancement of several orders of magnitude can be achieved mainly due to plasmonic effects. This bridges the gap between fluorescence and Raman spectroscopy and allows the investigation of single molecules with so called surface-enhanced Raman scattering (SERS).[4-6]

At present the only possibility to overcome the diffraction limit[7,8] with Raman spectroscopy requires the use of optical near-fields. Consequently, we will solely deal with the special properties of near-field Raman scattering[9-11], which luckily is

DOI: 10.1039/C5FD00031A

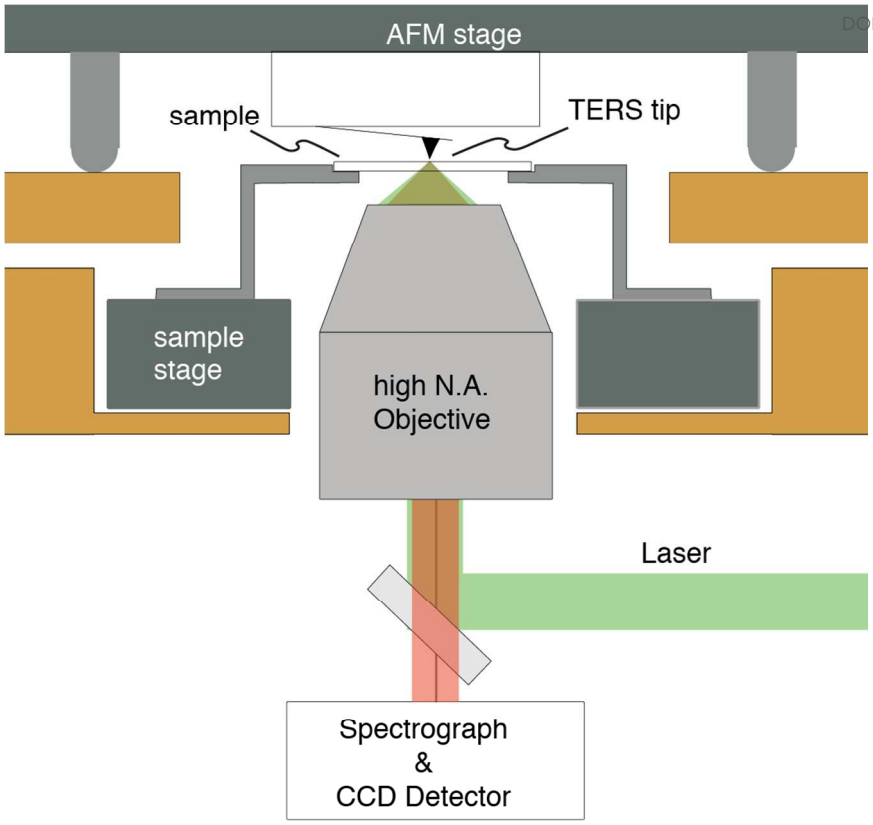

Figure 1: Schematic view of a TERS epi-illumination setup. Tip and sample can be scanned independently using precision piezo stages. Illumination and collection for the Raman system is done via a high N.A. objective. The detection of the Raman system is done after appropriate filtering using a standard multichromator / CCD detector arrangement.

in many ways directly associated with the aforementioned plasmonic effects. Accordingly a combination of near-field optics and SERS provides access to high lateral resolution, low detection limit, and high structural sensitivity. Furthermore, many aspects regarding the investigation of small sample volumes and thus restricted number of sampled molecules can be regarded as general aspects whenever such small dimensions are probed.

2 Experimental

General Setup

All investigations mentioned here were measured using a so-called tip-enhanced Raman scattering (TERS) setup. Figure 1shows the schematic sketch of our system. The main components are an atomic force microscope (AFM) and an inverted optical microscope equipped with a x,y,z piezo stage for automated sample scanning. The whole system is designed for a precise positioning of the near-field optical probe with respect to laser focus and sample. These parts are shown in dark

View Article Online
DOI: 10.1039/C5FD00031A

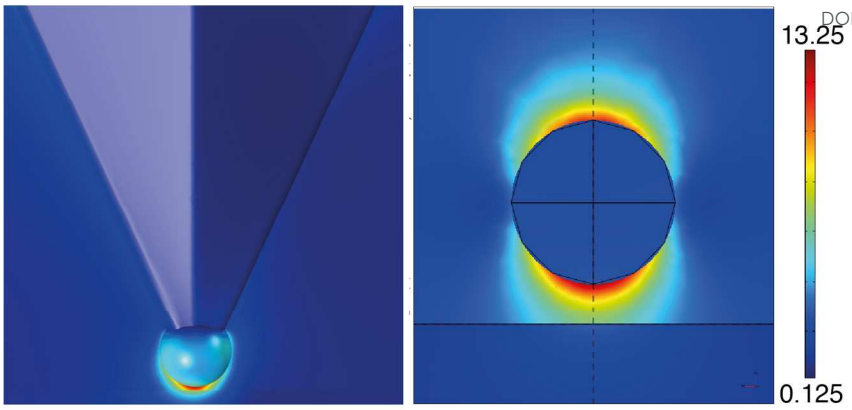

Figure 2: left panel: field distribution of an ideal TERS probe with one single nano particle attached to the apex of a AFM tip. Right panel detail of the field distribution E(x, z) using a dipol-mirror dipole model for a silver sphere radius 10 nm and a distance from the surface of 5nm, $\lambda = 413$ nm. Field distributions in both cases are comparable.

grey. Additionally, for coarse sample and tip alignment standard xy stages with ~2 µm precision are also available, but not shown in detail. Further details about this particular setup can be found in the literature where also a straightforward adaption to a reflection setup giving access to opaque samples is presented.[12-14]. The illumination through substrate and sample on to the plasmonic tip seems to be demanding and prone to losses, however, this setup allows for the best collection efficiency and implementing proper polarisation allows an optimal excitation of the nanoparticles.

TERS tips

Theory

The TERS tips are the integral element part of the entire system. Their special properties are responsible for the combination of high lateral resolution and signal enhancement. When irradiating silver or gold (other metals like Cu or Al have also been tested for special purposes) nanoparticles with light of an appropriate wavelength, electrons in the conducting band are collectively excited and oscillate with the same frequency as the incoming electromagnetic field. This can be considered as an optical analogue of a receiving antenna[15] and leads to an enhancement and confinement of the fields depending on shape and size of the actual nanoparticle. For details on the enhancement mechanism and a thorough theoretical description see Refs: [16-19]. In essence, if the experimental conditions are matched properly the field is confined to a very small volume close to the tip. Fig. 2 shows model calculations of "ideal" tips, either with a single nanoparticle on an AFM tip apex or even with only a single metal sphere. In both cases a total internal reflection illumination from the lower left was simulated. This results in an evanescent field excitation of the tip, which has some experimental advantages, but is not essential for such modelling. This geometry nevertheless explains the slight asymmetry of the electric field distribution. Most importantly, these simulations

View Article Online
DOI: 10.1039/C5FD00031A

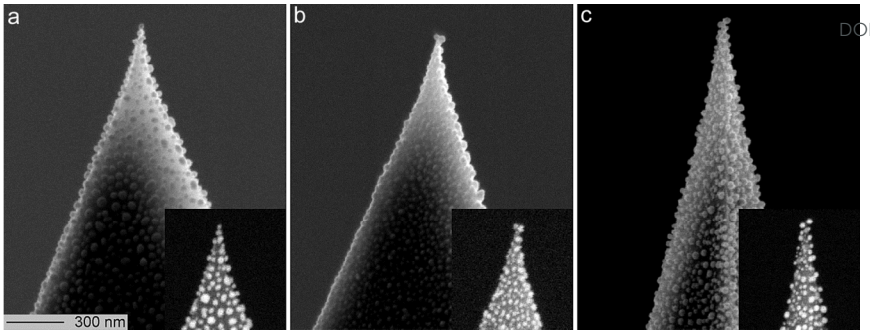

Figure 3: SEM images of the main manifestations of the silver nanoparticles on top of the TERS tips: a single nanoparticle at the outermost top (a), two nanoparticles at the top (b), or a single nanoparticle at the edge of the AFM tip (c), respectively. The scale bar applies to all images. The insets show the same tips using the material contrast.

reveal the extreme light confinement in all three dimensions. The main lateral enhancement is concentrated underneath the sphere with a size of roughly the radius of the particle. In focus direction the field decays even faster. As the Raman intensity scales approximately with the fourth power of the incident field a lateral resolution for realistic tip sizes (in our case 15-30 nm diameter) can be expected to be well below 5 nm. This value takes only into account the electromagnetic theory for the "macroscopic" appearance, specific atomic scale protrusions like corners or edges, as well as specific chemical interactions between the silver atoms and the sample, which both could potentially increase the resolution, are not considered. Interestingly, at very small scales below ~3Å quantum effects start to play a role, finally limiting the lateral resolution.[20] In any case one can expect a spatial resolution that renders many samples as single crystals or at least oriented in a statistically unexpected direction, if not special care is taken in sample preparation.

Tip Preparation

Fig. 3 shows typical SEM images of the tips mostly used in our group. These tips are obtained by physical vapour deposition of silver onto commercially available AFM tips[21] and the resulting silver nanoparticles have diameters of less than 30 nm. This approach is aimed to produce one more or less isolated small silver nanoparticle at the apex of the AFM tip and was initially developed for SERS substrates.[21-23] The nanoparticle at the tip apex serves as the active nano-antenna mentioned above. Inspecting more than hundred tip batches, three main geometries of the outermost silver nanoparticles were found. Type (a) reveals a single silver nanoparticle at the top of the AFM tip in close neighbourhood with other particles. Most of the time the nanoparticles are slightly off-axis. A second type (b) shows two silver nanoparticles at the top. Usually, one of the two nanoparticles is located a few nanometer in front of the other one. Thus, we can expect one acts as the plasmonically active device in the TERS experiment. About two thirds of our prepared tips fit to these two classes. Last but not least a small number of tips showed one clearly isolated front most silver nanoparticle, again usually slightly of axis (c). As the practical yield, e.g. ratio of tips in a batch that produce a considerable enhancement, of such tips is around 90% the actual geometry is influencing merely the details of the enhancement and, also quite important, the properties for the topographic sensing. Recently we

View Article Online
DOI: 10.1039/C5FD00031A

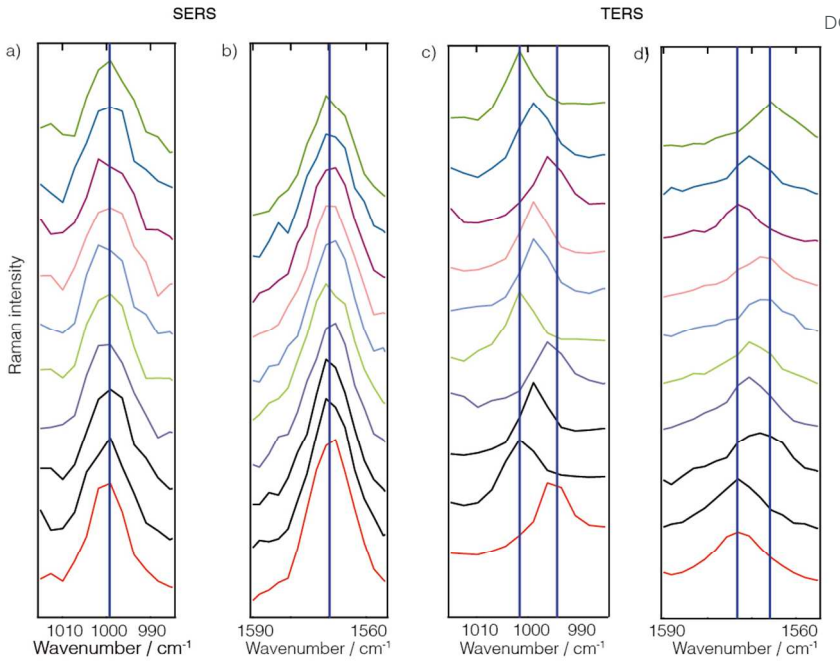

Figure 4: Comparison between SERS (a,b) and TERS (c,d) spectra of thiophenol monolayers. Due to the small number of molecules detected in the TERS case averaging effects like in the case of the SERS spectra are absent or not yet pronounced. This leads to stronger fluctuations in the TERS case.

successfully investigated a more directed approach for the particle attachment using dielectrophoresis.[24-28] This method allows to place single preselected nanoparticles onto an AFM cantilever, hence, seems to be promising for dedicated applications with preformed particles. Furthermore, many different approaches to tip production have been presented and it certainly depends on the specific experimental requirements, which type is suited best.[23,29-31 24,26-28,32]

Application examples

Self-assembled monolayers

In order to provide a reproducible way of sample preparation self-assembly is a well-established tool. This way only a single layer of molecules can be investigated and the orientation is generally predetermined. Certainly this approach is not feasible for most realistic samples, nevertheless, the study of self-assembled monolayers (SAM's) is ideal to rule out specific concentration effects. In particular if working with an extremely distance dependent method like TERS a layer such a thickness and orientation control is important to examine fundamental parameters. Several TERS studies were performed on molecules adsorbed onto gold single crystals.[29,30] This provides reliable conditions, as any surface roughness effects can be ruled out. In particular for STM based reflection TERS systems this is an ideal arrangement. In order to utilize the advantages of single crystalline surfaces for epi-illumination setups like the one shown in Fig. 3 methods were developed to manufacture gold[32-35] or silver[36,37] single crystals thin enough for the transmission of light. Those were readily applied to study small molecules like thiophenols, amino

View Article Online
DOI: 10.1039/C5FD00031A

acids and small peptides.[33,34,38,39] It became apparent, that in particular the spectra of aromatic amino acids monolayers lacked some usually strong bands, but could still be identified by other marker signals. If the experimental results were compared with theoretical models of amino acids on gold (111) surfaces it became evident, that due to the most favoured flat orientation of the molecules versus the surface the typical "ring breathing" modes were not efficiently excited in the TERS setup where the electric field vector is oriented orthogonally towards the surface and consequently orthogonal to the ring stretching vibrations.[36,40-43] Interestingly the field components at the tip side (see Fig. 2) did not play a role, as these components should have excited the supressed modes. This indirectly hints towards a high field confinement aka a high lateral resolution, which is of course difficult to determine on a SAM. To further study that effect an even simpler system was chosen.[38] Thiophenol was immobilized on flat and rough gold and silver surfaces. Here, the "ring breathing" mode was excited, as the perpendicular orientation of the molecule with respect to the surface is favourable for TERS excitation. The main target of the work was to study differences between SER and TER spectra of thiophenol monolayers. Often TERS signals tend to fluctuate slightly and the idea here was to control orientation and layer thickness as good as possible. Fig. 4 provides the most intriguing features of the experiments. The two spectra a and b on the left side show two selected SERS bands of a self-assembled thiophenol monolayer on a gold island film measured at arbitrary locations. The band parameters width, intensity, and spectral position hardly vary as can be expected if both, the film and the substrate, are homogeneous. The term "SERS substrate homogeneity" is a bit contradictory, as the substrates resemble more or less the silver island films on the AFM cantilevers shown in Fig. 3. On the other hand the laser spot is comparably large, and from the data it can be concluded that inhomogeneities of the films were averaged out. In this respect the corresponding TERS experiment should be even more reproducible: A ~30 nm thick gold flake, diameter 2-3 µm, and a surface roughness typically around 2Å is a much more regular sample support than any SERS substrate intrinsically can ever be. On top of this gold plate the TERS tip was positioned, whose enhancing properties hardly changed during the measurement. Still, the experimental data show much stronger band position fluctuations at different positions on the gold crystal compared to SERS (see Fig 4 c, d). A similar time dependent experiment over several minutes effectively showed the same behaviour for the SERS and TERS experiment, respectively. We attributed this behaviour to the fact that in the TERS experiment we probed such a small sample volume that averaging of minute molecule orientations was not observed, whereas in the SERS case much more molecules and also much more enhancing sites led to an effective averaging of the Raman signals. To support this hypothesis the band widths of the TERS and SERS experiments were also compared. Not surprisingly, the TERS data showed a broader distribution, however, the average width of the TERS experiments was always lower compared to the SERS spectra. As for both experiments the same physical constraints were applied, we hypothesise that the SERS spectra are a combination of many local single particles or single hot spot events, which would fundamentally resemble the TERS experiment. Besides, these results rises the question how many molecules are actually probed in a TERS experiment? Again a direct estimation of the resolution is not possible from a monolayer measurement, but it is certainly interesting to speculate on the number of molecules required for averaging effects dominating the spectra. For comparison, already hundred closely packed thiophenol

View Article Online
DOI: 10.1039/C5FD00031A

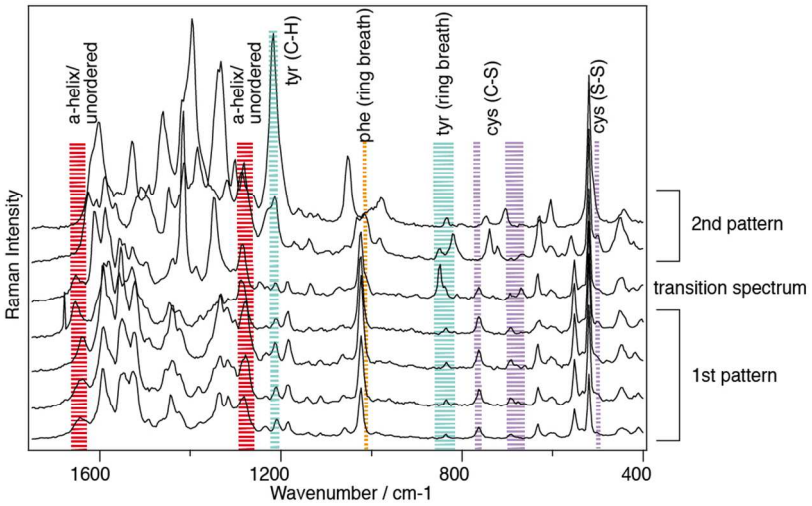

Figure 5: TERS spectra detected on an insulin amyloid protofilament generated at pH 1.5, laser excitation 532 nm, acquisition time 10s / spectrum, distance between positions 0.5 nm. Two major patterns can be clearly distinguished: only in the first 5 spectra α-helix/unordered structures can be clearly identified by amide I bands at 1640 cm^{-1}. A transition is also apparent in the synchronous appearance and disappearance of phenylalanine, tyrosine and cystine.

molecules fit approximately on a 4x4µm area.

Protein structures and spatial resolution

As a kind of by-product of our TERS investigations of protein structure surfaces, namely amyloid fibrils, the lateral resolution aspect emerged again. [40-44] When investigating fibrils with TERS using a step size of 5Å between subsequent positions, surprisingly pronounced spectral changes could be observed is the acquisition time was chosen long enough to allow a detailed band analysis. It should be mentioned here that Paulite et al. present TERS images of well-ordered amyloid nanotapes, that appear homogeneous. [45] Unfortunately the signal-to-noise ratio in those experiments was chosen such that apart from the phenylalanine "ring breathing" mode no other signal was detected and a prediction regarding structural changes are hardly possible. Hence, we consider the signal variations detected in our experiments as significant and related to the actual sample composition. If one considers furthermore the findings of the previous experimental and theoretical section concerning the lateral resolution, the chosen the step size of 5Å was set quite conservatively to avoid accidental undersampling of the dataset. When doing investigating the data we typically find results like shown in Fig. 5. Here we investigated an insulin amyloid protofilament and clearly see structural changes occurring on a length scale of a few Ångström. For instance, in the first five spectra one can observe an amide I band (at 1604 cm^{-1}) representing α-helix/unordered secondary structures. This is also observed, however slightly weaker, in the fifth spectrum, but then vanishes in the remaining two spectra. Similar patterns can be observed for the disappearance of the phenylalanine "ring breathing" mode and the appearance of a tyrosine marker band. The marker bands of cystine are also changing, however, as many different conformations around the disulfide bridge

View Article Online
DOI: 10.1039/C5FD00031A

affect the exact spectral position and intensity ratios of the associated bands, a full assignment would be too complex here. Similarly as detected in the self-assembled thiophenol monolayer case, one can observe similar spectral band position variations that are related to the immediate local environment of the sample. This can of course also involves the tip. These results can be simply understood as a way to investigate structural changes with high lateral resolution. But in fact this resolution is rather unexpected as we do not observe average peptide spectra, but rather locally dependent changes that reveal distinct amino acid contents.[44] Looking at the data of Fig. 4 and considering previous data on fibrils[41,42,44] and on DNA bases[46,47] a lateral resolution of about 1 nm can be estimated which actually is in the presented case at the limit of the sampling. Bearing in mind the TERS SAM experiments where a direct estimation of the resolution was not feasible, such a lateral resolution would relate to less than 10 molecules in the active region under the tip. For such a small number a "non-average" behavior becomes reasonable.

There is an important caveat to the generalization implied here. At the moment we are not aware of a full theoretical description that explains the lateral resolution of the experiments. It seems that either the size and shape parameters of the plasmonic tips have to be modeled differently, or that direct interactions of the tip and the sample provide an additional contrast that leads to the enhanced resolution observed. The later aspect is often termed "chemical enhancement" While currently strong efforts are made to unravel this issue, we think that any high resolution beyond 3-5 nm can be utilized to sequence virtually any material.

General method for sequencing a single strand

For such sequencing we will provide the outline of this method and an estimation of the precision that is required for a successful application.[48] One can consider a tip as a simple point dipole with the dipole in z-direction with a given field distribution that results in a TERS interaction volume as mentioned previously. This means for the following ideas we assume the theoretically predicted lateral resolution values and not even the values we experimentally determined. If, for instance a DNA single strand is aligned along the x-axis with bases at the positions x_k (k = 1, 2, …, K) and z = 0, and the tip moves along x at the height z, the signal at position x_n for one particular Raman peak will be

$$S(x_n) = \sum_{k=1}^{K} b_k \, P(x_n - x_k, z), \qquad n = 1 \ldots N$$

b_k equals either 1 or 0, depending on whether the regarded monomer (here nucleobase) is present at x_k (or not). P(x,z) is related to the influence of the tip and is proportional to the 4th power of the field. For N > K the coefficients b_k can be calculated using a least square fitting method that requires the inversion of the matrix (M).

$$M_{lk} = \sum_{n=1}^{N} P(x_n - x_k, z) \; P(x_n - x_l, z), \qquad k, l = 1 \ldots K$$

Such inverse problems are often ill conditioned, i.e. a small error in the input values ($S(x_n)$) can result in huge errors in the reconstructed solution (b_k). A useful method to evaluate this problem is the singular value decomposition of the matrix M which

DOI: 10.1039/C5FD00031A

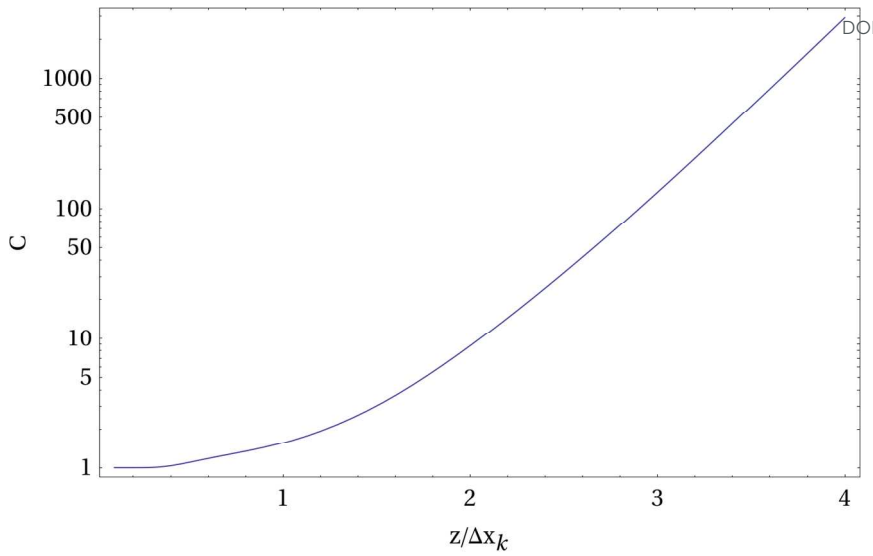

Figure 6: Condition number C of the inverse sequencing problem using the theoretically modeled enhancement profile of a TERS tip. The graph shows how quickly the methods gets unreliable if the distance z between tip and sample increases. The x-axis values represent normalized distances normalized to a single unit of interest Δx_k (for instance a base-to-base distance in DNA). Interestingly an AFM can achieve the required small distances.

provides the condition number C. This number allows the estimation of the error of the reconstructed b values for a given error ΔS/S of the actually measured signal S

$$\frac{\Delta b}{b} \leq C \frac{\Delta S}{S}$$

Fig. 6 shows the condition number of our problem as a function of the distance between tip dipole and base size normalized with respect to the base-to-base distance. We assumed 5 samples per base, i.e. N = 5 K, in other words, the polymer strand is scanned in such a way that each single base is sampled at five different subsequent TERS tip positions. The data show that a direct reconstruction of the b_k values is only possible for extremely small distances between the bases in the DNA strand and the tip dipole which corresponds to the center of the Ag sphere in the experiment. If, for example, the error in the Raman signal is 1 % this estimation results in a maximum distance z of two base-to-base distances corresponding to roughly 1 nm. In addition to this general estimation we performed simulations where we started with several arbitrary base arrangements and calculated the corresponding TERS signal. After adding a certain noise to the signal we recalculated the base positions. The simulations show that slightly higher distances are allowed compared with the estimation given above, but the general trend was confirmed. While this renders the sequencing a challenging problem, it is also clear that the method's quality will improve dramatically with improving lateral resolution. Taking into account the experimental resolution value estimations a direct sequencing as proposed already in the first TERS paper on DNA strands[49] is possible.

View Article Online
DOI: 10.1039/C5FD00031A

Conclusion

We presented the high resolution aspects of Raman spectroscopy using different approaches. By studying homogeneous samples under controlled conditions, a comparison of signal position fluctuations indicates that TERS probes very small sample volumes where individual orientation effects are not averaged. Complementary studies on proteins and protein fibrils reveal a surprising capability to distinguish amino acid distributions locally on a length scale of at least 1 nm, also confirming the high spatial resolution of TERS. Interestingly, no consistent theory is at hand to explain this resolution with usual approach using the "macroscopic" tip parameters. Last not least we present a general method that allows a direct sequencing of single polymer stands with TERS that already would work with the current theoretically predicted resolution.

The time resolution aspects of TERS have not been addressed here, but are currently investigated successfully by the van Duyne group[50]. This way the goal to combine ultimate temporal, spatial and spectral resolution as a general tool should be reached I the to too far future.

Acknowledgement

We gratefully acknowledge support from the Deutsche Forschungsgemeinschaft (FR 1348/19-1) the Alexander von Humboldt foundation, the Carl-Zeiss Foundation and the Thüringer Aufbaubank (FKZ: 2011 FE 9048; 2011 VF 0016) for their financial support.

References

[a] *Leibniz Institute of Photonic Technology, Albert-Einstein-Str. 9, 07745 Jena, Germany. Fax: 0049 3641 206 139 Tel: 0049 3641 206 139; E-mail: Volker.deckert@ipht-jena.de*
[b] *Institute of Physical Chemistry and Abbe Center of Photonics,University of Jena, Helmholtzweg 4, 07743 Jena, Germany.*

1. M. Fleischmann, P. Hendra, and A. McQuillan, *Chem Phys Lett*, 1974, **26**, 163–166.
2. M. G. Albrecht and J. A. Creighton, *J Am Chem Soc*, 1977, **99**, 5215–5217.
3. D. Jeanmaire and R. van Duyne, *J Electroanal Chem*, 1977.
4. S. Nie and S. Emory, *Science*, 1997.
5. K. Kneipp, Y. Wang, H. Kneipp, L. Perelman, and I. Itzkan, *Phys Rev Lett*, 1997.
6. E. C. Le Ru, M. Meyer, and P. G. Etchegoin, *The journal of physical chemistry B*, 2006, **110**, 1944–1948.
7. E. Abbe, *Archiv f. mikrosk. Anatomie*, 1873, **9**, 413–418.
8. Rayleigh, *The London, Edinburgh, and Dublin Philosophical Magazine and Journal of Science*, 1879, **8**, 261–274.
9. D. A. Smith, S. Webster, M. Ayad, S. D. Evans, D. Fogherty, and D. Batchelder, *Ultramicroscopy*, 1995, **61**, 247–252.
10. C. L. Jahncke, H. D. Hallen, and M. A. Paesler, *J Raman Spectrosc*, 1996, **27**, 579–586.
11. D. Zeisel, B. Dutoit, V. Deckert, T. Roth, and R. Zenobi, *Anal Chem*, 1997, **69**, 749–754.
12. A. Rasmussen and V. Deckert, *J Raman Spectrosc*, 2006, **37**, 311–317.
13. E. Bailo and V. Deckert, *Chem. Soc. Rev.*, 2008, **37**, 921–930.
14. T. Deckert-Gaudig, M. Richter, D. Knebel, T. Jähnke, T. Jankowski, E. Stock, and V.

View Article Online
DOI: 10.1039/C5FD00031A

Deckert, *Appl Spectrosc*, 2014, **68**, 916–919.
15. L. Novotny and B. Hecht, 2012.
16. M. Moskovits, *Reviews of Modern Physics*, 1985.
17. M. Kerker, *SPIE milestone series*, 1990, **10**, XIX–696 p.
18. A. Otto, I. Mrozek, H. Grabhorn, and W. Akemann, *J Phys-Condens Mat*, 1992, **4**, 1143–1212.
19. H. Kim, K. M. Kosuda, R. P. van Duyne, and P. C. Stair, *Chem. Soc. Rev.*, 2010, **39**, 4820–4844.
20. K. J. Savage, M. M. Hawkeye, R. Esteban, A. G. Borisov, J. Aizpurua, and J. J. Baumberg, *Nature*, 2012, **491**, 574–577.
21. R. Stockle, Y. Suh, V. Deckert, and R. Zenobi, *Chem Phys Lett*, 2000, **318**, 131–136.
22. R. Stockle, V. Deckert, C. Fokas, and R. Zenobi, *Appl Spectrosc*, 2000, **54**, 1577–1583.
23. N. Hayazawa, Y. Inouye, Z. Sekkat, and S. Kawata, *Opt Commun*, 2000, **183**, 333–336.
24. B. Ren, G. Picardi, and B. Pettinger, *Rev Sci Instrum*, 2004, **75**, 837–841.
25. C. Leiterer, T. Deckert-Gaudig, P. Singh, J. Wirth, V. Deckert, and W. Fritzsche, *Electrophoresis accepted*.
26. G. Xu, Z. Liu, K. Xu, Y. Zhang, H. Zhong, Y. Fan, and Z. Huang, *Rev Sci Instrum*, 2012, **83**.
27. P. R. Brejna and P. R. Griffiths, *Appl Spectrosc*, 2010, **64**, 493–499.
28. T. Kim, K.-S. Jeon, K. Heo, H. M. Kim, J. Park, Y. D. Suh, and S. Hong, *Analyst*, 2013, **138**, 5588–5593.
29. B. Pettinger, B. Ren, G. Picardi, R. Schuster, and G. Ertl, *Phys Rev Lett*, 2004, **92**, 096101.
30. B. Ren, G. Picardi, B. Pettinger, R. Schuster, and G. Ertl, *Angew Chem Int Edit*, 2005, **44**, 139–142.
31. R. D. Rodriguez, E. Sheremet, S. Müller, O. D. Gordan, A. Villabona, S. Schulze, M. Hietschold, and D. R. T. Zahn, *Rev Sci Instrum*, 2012, **83**, 123708–123708.
32. T. Deckert-Gaudig and V. Deckert, *Small*, 2009, **5**, 432–436.
33. T. Deckert-Gaudig and V. Deckert, *J Raman Spectrosc*, 2009, **40**, 1446–1451.
34. T. Deckert-Gaudig, E. Bailo, and V. Deckert, *Physical chemistry chemical physics : PCCP*, 2009, **11**, 7360–7362.
35. J.-S. Huang, V. Callegari, P. Geisler, C. Brüning, J. Kern, J. C. Prangsma, X. Wu, T. Feichtner, J. Ziegler, P. Weinmann, M. Kamp, A. Forchel, P. Biagioni, U. Sennhauser, and B. Hecht, *Nat Commun*, 2010, **1**, 150.
36. T. Deckert-Gaudig, E. Rauls, and V. Deckert, *J Phys Chem C*, 2010, **114**, 7412–7420.
37. T. Deckert-Gaudig, F. Erver, and V. Deckert, *Langmuir*, 2009, **25**, 6032–6034.
38. P. Singh, T. Deckert-Gaudig, H. Schneidewind, K. Kirsch, E. M. van Schrojenstein Lantman, B. M. Weckhuysen, and V. Deckert, *Phys Chem Chem Phys*, 2015, **17**, 2991–2995.
39. E. M. van Schrojenstein Lantman, T. Deckert-Gaudig, A. J. G. Mank, V. Deckert, and B. M. Weckhuysen, *Nat Nanotechnol*, 2012, **7**, 583–586.
40. A. V. Krasnoslobodtsev, A. M. Portillo, T. Deckert-Gaudig, V. Deckert, and Y. L. Lyubchenko, *Prion*, 2010, **4**, 265–274.
41. D. Kurouski, T. Deckert-Gaudig, V. Deckert, and I. K. Lednev, *J Am Chem Soc*, 2012, **134**, 13323–13329.
42. M. Schleeger, C. C. vandenAkker, T. Deckert-Gaudig, V. Deckert, K. P. Velikov, G. Koenderink, and M. Bonn, *Polymer*, 2013, **54**, 2473–2488.
43. D. Kurouski, T. Deckert-Gaudig, V. Deckert, and E. al, *Biophys J*, 2014, **106**, 263–271.
44. T. Deckert-Gaudig, E. Kämmer, and V. Deckert, *J. Biophoton.*, 2012, **5**, 215–219.
45. M. Paulite, C. Blum, T. Schmid, L. Opilik, K. Eyer, G. C. Walker, and R. Zenobi, *ACS Nano*, 2013.
46. R. Treffer, X. Lin, E. Bailo, T. Deckert-Gaudig, and V. Deckert, *Beilstein J Nanotechnol*, 2011, **2**, 628–637.
47. R. Treffer, R. Böhme, T. Deckert-Gaudig, K. Lau, S. Tiede, X. Lin, and V. Deckert, *Biochem. Soc. Trans.*, 2012, **40**, 609–614.
48. V. Deckert and M. Zeisberger, *register.dpma.de*, 2013.
49. E. Bailo and V. Deckert, *Angew Chem Int Ed Engl*, 2008, **47**, 1658–1661.
50. J. M. Klingsporn, M. D. Sonntag, T. Seideman, and R. P. van Duyne, *The Journal of Physical Chemistry Letters*, 2014, **5**, 106–110.